Macromolecules

pubs.acs.org/Macromolecules Article

Monitoring the Formation of Polymer Nanoparticles with Fluorescent Molecular Rotors

Sascha Schmitt, Galit Renzer, Jennifer Benrath, Andreas Best, Shuai Jiang, Katharina Landfester, Hans-Jürgen Butt, Roberto Simonutti,* Daniel Crespy,* and Kaloian Koynov*

Cite This: *Macromolecules* 2022, 55, 7284–7293 Read Online

ACCESS | Metrics & More | Article Recommendations | Supporting Information

ABSTRACT: We present an experimental approach to studying the kinetics of polymer nanoparticle formation using molecular rotor molecules as fluorescence probes. By combining fluorescence lifetime analysis and fluorescence correlation spectroscopy, it is possible to simultaneously monitor the evolution of the local environment in the nanoparticles and their size. To assess the generality of the method, we select two common but very different methods for nanoparticle preparation: emulsion-solvent evaporation and miniemulsion polymerization. In both cases, three stages of the nanoparticle formation process were identified on the basis of their polymer content. In the initial stage of the process, the polymer content is low. Then it increases rapidly because of solvent evaporation or polymerization during the second stage. Finally, it reaches a plateau value. Furthermore, significant heterogeneities in the final nanoparticles were found that can be attributed to remaining solvent or monomer and the spatial variation of the polymer-free volume.

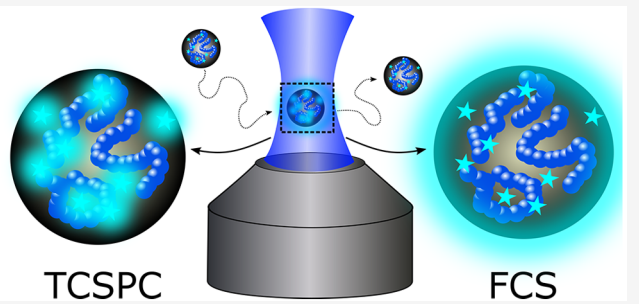

1. INTRODUCTION

Polymeric nanoparticles are nowadays used in many applications because of their high surface area and versatility for surface functionalization. They have hence been employed as sensors,[1−5] catalysts,[6,7] and drug delivery systems,[8−10] implemented in other materials for energy conversion and storage,[11] and used as building blocks for fabricating suprastructures, colloidal crystals, and coatings.[12−16]

Although there is a cornucopia of methods for preparing polymer nanoparticles, the real-time monitoring of their formation is still a challenge. While spectroscopic or calorimetric methods allow for a determination of the polymerization rate or conversion, it is difficult to obtain information about the morphology and local viscosity *within* nanodroplets and nanoparticles.

Herein, we prepared and monitored polymer nanoparticles via two common but very different methods, which are the emulsion-solvent evaporation and the miniemulsion polymerization processes.[17] The first method relies on the emulsification of polymer solutions followed by the evaporation of a solvent present in the dispersed phase.[18] In miniemulsion polymerization, monomer droplets are converted to polymer nanoparticles by a polymerization reaction.[19] Whereas the stabilization mechanism is now well understood for both processes,[20−23] there is still a lack of information regarding the evolution of the local environment inside the liquid droplets when they are converted to solid nanoparticles, especially in the case of particles with complex morphologies. A major reason is the lack of experimental approaches that can provide local information not only on the size but also on the internal morphology and structure of very small nanodroplets and nanoparticles diffusing in a continuous liquid phase. In this context, we explore here the possibility of using tailored fluorescent molecules, called molecular rotors, as reporters simultaneously providing local information on the evolution of both the structure of the nanodroplets/nanoparticles and their size.

The term "rotor" refers to the formation upon excitation of an intramolecular twisting between at least two rigid molecular portions along the σ-bond that connects them. They typically consist of an electron-donating and an electron-accepting subunit spaced by a conjugated spacer. The latter ensures electron transfer from donor to acceptor but prevents orbital overlap between the two; when the molecule is photoexcited, a donor-to-acceptor charge transfer occurs, and a rotation of a subunit relative to the other is induced by electrostatic forces. This nonemissive twisted intramolecular charge transfer (TICT) state can then relax by (i) adiabatic transition to an emissive state or (ii) nonradiative relaxation by untwisting. If

Received: June 1, 2022
Revised: July 20, 2022
Published: August 11, 2022

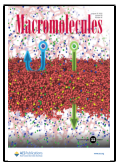

https://doi.org/10.1021/acs.macromol.2c01132
Macromolecules 2022, 55, 7284−7293

the local viscosity is high, then intramolecular rotations are hampered and the probability of nonradiative relaxation is reduced, resulting in longer luminescence lifetimes and higher quantum yields.[24−28] Thus, molecular rotors were successfully used in various applications ranging from intracellular viscosity imaging[28−32] to monitoring block copolymer micelle formation[33] or polymerization processes.[34−36] When fluorescent rotor molecules are added to the organic phase during polymeric nanoparticle preparation from emulsion droplets, their lifetime can be continuously measured and used to monitor changes in the local mobility within the nanodroplet/nanoparticle and thus in their polymer content and inner morphology.

At the same time, the fluorescence signal of the molecular rotors can be used to monitor changes in the size of the nanodroplets/nanoparticles during the formation process by fluorescence correlation spectroscopy (FCS). In an FCS experiment, the fluorescence intensity fluctuations caused by fluorescent species dispersed in a fluid medium and diffusing through a very small (<1 μm^3) observation volume, typically the "focus" of a confocal microscope, are recorded and analyzed by autocorrelation analysis. This yields information on the hydrodynamic radius, fluorescence brightness, and concentration of the studied fluorescent species. These species can be single dye molecules, fluorescent (or labeled) macromolecules, or nanoparticles. In the last two decades, FCS has become an important tool in polymer and colloid science.[37−45] Furthermore, the method has been successfully used to quantify the evolution of nanodroplet/nanoparticle size and study the process of droplet coalescence during the formation of nanoparticles by miniemulsion polymerization and the emulsion-solvent evaporation methods.[20,21]

Here, we explored the possibility of using a molecular rotor as a fluorescent reporter, simultaneously providing information on the polymer content inside polystyrene nanoparticles and their size during the formation process. Two commonly used synthesis strategies for nanoparticle preparation, namely, solvent evaporation from emulsion droplets and miniemulsion polymerization, were tested. Time-correlated single photon counting (TCSPC) and fluorescence correlation spectroscopy were used to simultaneously measure the fluorescence lifetime of the molecular rotors and the hydrodynamic radius of the forming nanoparticles, respectively.

2. MATERIALS AND METHODS

2.1. Materials. Styrene (≥99.5%) was purchased from Carl Roth and purified on a column packed with neutral Al_2O_3 (50−200 μm, 60 Å, Acros Organics) before use. Anhydrous hexadecane and azobis(isobutyronitrile) (≥98.0%) were purchased from Sigma-Aldrich. Toluene (≥99.8%) was purchased from Fisher Scientific, and sodium dodecyl sulfate (SDS, ≥99%) was purchased from Acros Organics. The fluorescent dye Atto425 was purchased from Atto-Tec GmbH (Siegen, Germany). Polystyrene (PS, M_w = 60 kg/mol, $Đ$ = 1.03) was synthesized by anionic polymerization, initiated by *sec*-butyllithium. The fluorescent molecular rotor AzeNaph1 was a kind donation from Prof. L. Beverina.

2.2. Solutions of PS in Toluene or Styrene. Solutions with a predefined polystyrene content in toluene or styrene were produced as follows. PS (M = 60 kg mol^{-1}) fractions of 10 to 50 wt % were dissolved independently in the respective solvent containing the molecular rotor (c = 10^{-6} M). The solutions were stirred for 1 day before the fluorescence lifetime measurements. Solutions with a polystyrene fraction of more than 50 wt % cannot be prepared in this way because their viscosity is too high to obtain a homogeneous solution through stirring. Therefore, solutions with higher polymer fractions were obtained by evaporating the respective solvent from a 50 wt % sample. The actual polystyrene fraction was then calculated on the basis of the weight loss. The samples were dried in an oven (without vacuum) at 70 °C and then weighed to calculate the PS content. By repeating this step, it was possible to obtain polymer fractions of up to 95 wt %. The solutions were placed in an Attofluor cell chamber, and the fluorescence lifetime measurements were performed at room temperature.

2.3. Preparation of PS Films. Drop-cast PS films were prepared by dissolving 50 mg of PS (M = 60 kg mol^{-1}) in 200 μL of toluene containing the molecular rotor AzeNaph1 (c = 10^{-6} M). A 50 μL solution was deposited on a glass slide and dried overnight at 80 °C under reduced pressure. The last step was performed in order to remove the residual solvent that may be left in thin films,[46] which could have affected the behavior of the molecular rotors.

Spin-coated PS films with a thickness of around 500 nm were prepared by dissolving 15.6 mg of PS in 282 μL of toluene containing the molecular rotor AzeNaph1 (c = 10^{-5} M). This solution (150 μL) was then spin-coated on a thin (150 μm) glass slide (30 s at 2000 rpm) and subsequently dried overnight under reduced pressure at 80 °C to remove residual solvent.

2.4. Preparation of Nanoparticles by the Emulsion-Solvent Evaporation Method. An aqueous SDS solution (20 g, 1 g/L) was added to a solution of PS (50 mg) in 1.44 mL of toluene containing the molecular rotor AzeNaph1 (c = 10^{-6} M) and stirred for 1 h at room temperature. The obtained macroemulsion was sonicated using a Branson W450-D sonifier with a $^1/_2$-inch tip at 90% amplitude for 120 s under ice cooling. After the sonification, the solution was transferred to a 50 mL round-bottomed flask and stirred at 500 rpm for 8 h at 40 °C. During this period, aliquots (∼250 μL) were taken at certain time intervals and investigated by FCS and fluorescence lifetime experiments.

2.5. Synthesis of Nanoparticles by Miniemulsion Polymerization. Styrene (6 g) containing the molecular rotor AzeNaph1 (c = 10^{-6} M) was mixed with 300 mg of hexadecane and 100 mg of AIBN. To the organic phase, 24 g of an aqueous solution of SDS (c = 2.8 g/L) was added and stirred for 1 h at room temperature. The macroemulsion was sonicated using a Branson W450-D sonifier with a $^1/_2$-inch tip at 90% amplitude for 120 s under ice cooling. After the sonification, the miniemulsion was transferred to a 50 mL round-bottomed flask and stirred for 12 h at 72 °C. Aliquots (∼250 μL) were taken at certain time intervals and studied by FCS and fluorescence lifetime experiments.

2.6. Analytical Tools. Fluorescence lifetime and FCS experiments were performed on an LSM880 confocal microscope (Carl Zeiss, Jena, Germany) equipped with a FLIM and an FCS upgrade kit (PicoQuant, Berlin, Germany). The excitation was performed with a 405 nm diode laser (LDH-D-C-405, PicoQuant, Berlin, Germany) fiber coupled to the microscope. The excitation light was collimated, reflected by an MBS405 dichroic mirror (Carl Zeiss, Jena, Germany), and focused into the studied samples by a Zeiss C-Apochromat 40×/1.2 W water-immersion objective. The focus was positioned only 20 μm deep in the studied samples to minimize aberations caused by the refractive index mismatch between the immersion liquid (water) and the sample media (e.g., an aqueous dispersion of NPs). The fluorescent light was collected with the same objective, passed through a pinhole and a band-pass filter EM525/50 (Chroma, Technology, Vermont, USA), and directed to a SPAD detector (PDM, Micro Photon Devices, Bolzano, Italy) connected to a TCSPC board (TimeHarp 260, PicoQuant, Berlin, Germany).

The recorded TCSPC data were evaluated using the PicoQuant SymPhoTime 64 software. Fluorescence decay curves were fitted with either a monoexponential or biexponential function, i.e., n = 1 or 2 in eq 1.

$$I(t) = \sum_{i=1}^{n} A_i e^{(-t/\tau_i)} \quad (1)$$

https://doi.org/10.1021/acs.macromol.2c01132
Macromolecules 2022, 55, 7284−7293

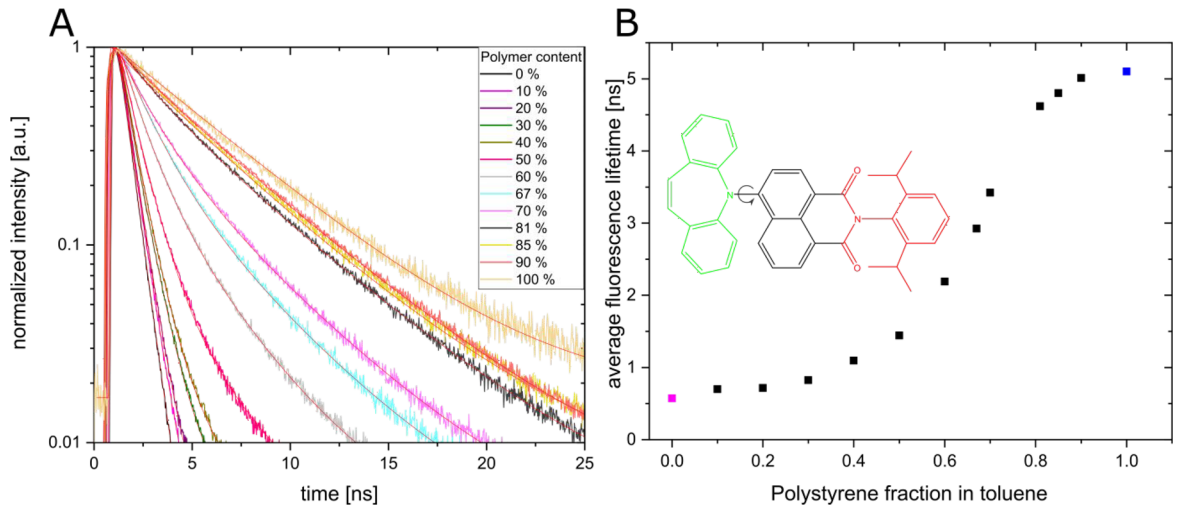

Figure 1. (A) Typical fluorescence decay curves of the molecular rotor AzeNaph1 in toluene solutions of polystyrene. The solid lines represent the respective fits with eq 1. (B) Weighted-average fluorescence lifetime of AzeNaph1 versus the polystyrene concentration. The single fluorescence lifetimes measured in toluene (magenta) and a dry polystyrene film (blue) are also shown for comparison. (Inset) Structure of AzeNaph1; green, dibenzo[b,f]azepine, electron-rich group (donor); black, electron-poor naphthaleneimide unit (acceptor) connected by a single −C−N− bond that allows for intramolecular rotation (indicated by the arrow).

Here, A_i and τ_i denote the amplitude and the lifetime of the ith component, respectively. If the decay curve possesses two lifetimes, then the weighted-average lifetime was also calculated as follows:

$$\tau_{Av} = \frac{\sum_{i=1}^{2} A_i \cdot \tau_i}{\sum_{i=1}^{2} A_i} \quad (2)$$

FCS data were recorded simultaneously on the same LSM880 setup. The fluorescent light was detected in the range of 500−553 nm with the microscope's inbuilt 32-channel GaAsP photomultiplier array (QUASAR, Carl Zeiss, Jena, Germany) operating in photon counting mode. The experimental autocorrelation curves originating from the nanoparticles (or nanodroplets) diffusing through the observation volume were fitted with the Zeiss ZEN software using the analytic equation for an ensemble of m types of freely diffusing species:

$$G(\tau) = 1 + \left[1 + \frac{f_T}{1 - f_T} e^{-\tau/\tau_T}\right] \frac{1}{N} \sum_{i=1}^{m} \frac{f_i}{\left[1 + \frac{\tau}{\tau_{D,i}}\right] \sqrt{1 + \frac{\tau}{S^2 \tau_{D,i}}}} \quad (3)$$

Here, f_T and τ_T are the fraction and the decay time of the triplet state, and N denotes the average number of fluorescent species in the observation volume during an FCS measurement. In our experiment, N was around 10. f_i is the fraction of the fluorescent species possessing the diffusion time $\tau_{D,i}$. The so-called structure factor S (around 6 in our experiments) represents the quotient of the axial and radial dimensions of the confocal volume $S = z_0/r_0$. The diffusion coefficient D_i of the ith species was evaluated from their diffusion time through

$$D_i = \frac{r_0^2}{4\tau_{D,i}} \quad (4)$$

From the diffusion coefficient, the respective hydrodynamic radius R_H was calculated through the Stokes−Einstein relation as

$$R_H = \frac{k_B T}{6\pi\eta D} \quad (5)$$

Here, T is the absolute temperature, k_B is the Boltzmann constant, and η is the viscosity of the solvent. Because the value of r_0 depends strongly on the specific characteristics of the optical setup, calibration experiments were performed using a fluorescent tracer with a known diffusion coefficient, i.e., Atto425 in water.

It should be noted that the fluorescent brightness of the molecular rotors increases roughly 10-fold when their environment changes from low-polymer-content nanodroplets to high-polymer-content nanoparticles. Thus, the excitation light intensity was tuned using gray filters in order to keep the detected fluorescence light intensity relatively constant.

3. RESULTS AND DISCUSSION

3.1. Molecular Rotor. The molecular rotor selected for this study (AzeNaph1,[33] Figure 1B inset) consists of an electron-donating and rigid dibenzoazepine residue linked to an electron-deficient naphthalene imide residue. In comparison to most commercially available molecular rotors[26,47,48] that either are designed for aqueous environments or are at least partially water-soluble (e.g., BODIPY,[27,48] 9-(dicyanovinyl)-julolidine (DCVJ),[47] thioflavin, or 2-(4-(dimethylamino)-benzyl-idene)malo-nitrile[49]), AzeNaph1 has negligible water solubility.[33] Indeed, it was crucial that the molecular rotor was soluble only in the dispersed organic phase of emulsions to provide unambiguous information about its location. Furthermore, AzeNaph1 displays a high (∼70 nm) Stokes shift, stability, and a fluorescence lifetime that is strongly dependent on the viscosity of the environment, ranging from less than 1 ns in pure organic solvents to up to 5−8 ns in solid polymer films.[33]

We first investigated the behavior of this molecular rotor in polymer solutions with well-defined concentrations. Figure 1A shows fluorescence decay curves measured by TCSPC in toluene solutions of polystyrene (M_w = 60 kg mol^{-1}) with different concentrations. With the increase in polystyrene fraction in the solvent, the curves exhibit a clear shift to longer decay times, reflecting the increasing viscosity of the local environment of the molecular rotor. Furthermore, curves measured in pure toluene (0% polymer content) and in dry polystyrene films (100% polymer content, blue symbols) are also shown for comparison. Both curves can be fitted with a monoexponential decay (n = 1 in eq 1), meaning that all molecular rotors experience a similar local environment in these media. The fits yielded corresponding fluorescence lifetimes for AzeNaph1 of τ_{tol} = 0.57 ns in toluene and $\tau_{PS\ film}$ =

https://doi.org/10.1021/acs.macromol.2c01132
Macromolecules 2022, 55, 7284−7293

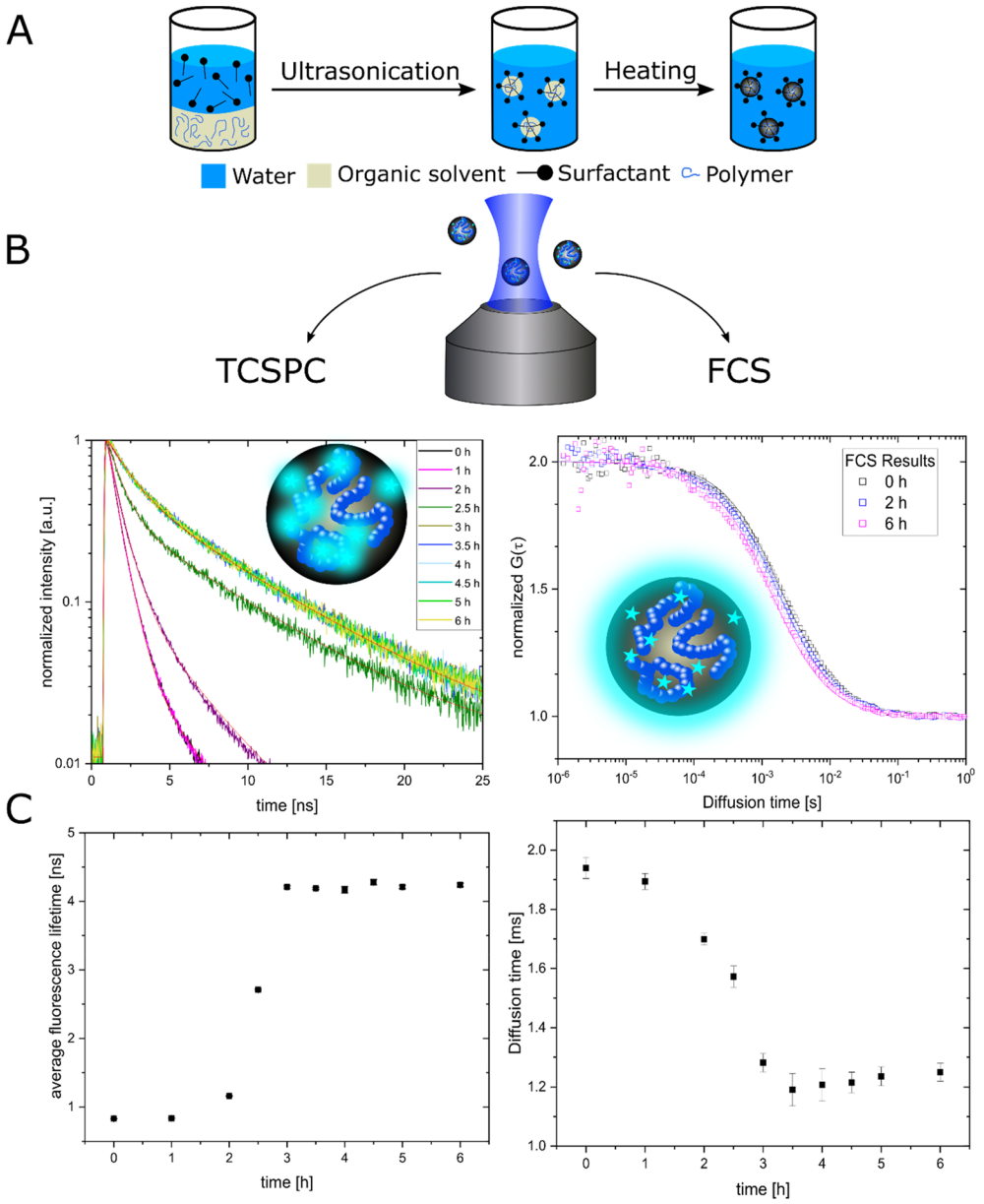

Figure 2. (A) Schematic overview of the emulsion-solvent evaporation process. (B) Working principle of using the molecular rotor as a reporter providing information on both the inner viscosity and the size of the polystyrene nanoparticles during their formation. The fluorescence of the individual molecular rotor molecules is used to record fluorescence decay curves by TCSPC (left side), whereas the fluorescence of the whole nanoparticle is used to record FCS autocorrelation curves (right side). (C) Average fluorescence lifetime of AzeNaph1 (left) and nanoparticles' diffusion times (right) vs the time of the emulsion-solvent evaporation process (heating time). The size of the error bars for the fluorescence lifetime are comparable to the symbol size.

5.2 ns in dry polystyrene films. In contrast, the fluorescence decay curves measured in the polystyrene solutions required a biexponential fitting ($n = 2$ in eq 1), yielding two fluorescence lifetimes: short τ_1 and long τ_2 and their respective amplitudes A_1 and A_2. At a low polymer concentration, τ_1 is similar to τ_{tol} measured in pure toluene, and τ_2 is significantly longer and at high polymer concentration approaches the value of τ_{PS} measured in dry polystyrene films (Figure S1). These findings highlight the nonhomogeneous nature of the polymer solutions on the length scale of the molecular rotor molecules (~1 nm) and indicate that during a TCSPC experiment some of these molecules are located in a solvent (toluene)-rich environment and others are located in a polymer-rich environment. The amplitudes of the two decay processes A_1 and A_2 represent the fractional number of rotor molecules in each environment. Although it is obvious that A_1 decreases and A_2 increases with increasing polymer concentration (Figure S1), it should be noted that both τ_1 and τ_2 increase with increasing polymer concentration. This means that the local viscosity is increasing not only in the polymer-rich environment but also to some extent in the solvent-rich environment. Furthermore, neither the polymer-rich nor the solvent-rich environments are completely homogeneous; therefore, the use of biexponential fits is the simplest possible representation. Both τ_1 and τ_2 are hence average values of the various lifetimes that the rotors display in the solvent-rich and polymer-rich environments.

Moreover, the weighted-average fluorescence lifetimes of AzeNaph1 in the polystyrene solutions were evaluated using eq

https://doi.org/10.1021/acs.macromol.2c01132
Macromolecules 2022, 55, 7284−7293

2 and plotted in Figure 1B together with the single-exponential decay lifetimes measured in pure toluene (magenta symbol) and in dry PS films (blue symbol). The rotor fluorescence lifetime increased monotonically with the PS fraction.

3.2. Polymer Nanoparticles Prepared by the Emulsion-Solvent Evaporation Method. The emulsion-solvent evaporation process is an important method for preparing polymer nanoparticles (Figure 2A).[18] The method relies on the emulsification of a polymer solution, usually in an aqueous continuous phase, followed by the evaporation of the solvent present in the dispersed phase to obtain polymer nanoparticles. The formation of hydrophilic nanoparticles dispersed in an apolar continuous phase has also been reported, although rarely.[50] Herein, AzeNaph1 and PS were dissolved in toluene and emulsified in an aqueous solution of SDS to form a miniemulsion. The miniemulsion was then heated to evaporate toluene, taking advantage of the water−toluene azeotrope, to form solid PS nanoparticles dispersed in water.

Aliquots of the miniemulsion were taken at regular time intervals (0, 1, 2, 3, 4, 5, and 6 h) after ultrasonication and during the evaporation of toluene and were studied with TCSPC and FCS. Figure 2B illustrates how the molecular rotors dispersed in the nanodroplets were used as fluorescent reporters providing information on both the local viscosity in the droplets (left side) and their size (right side) during the emulsion-solvent evaporation process. In the TCSPC experiments, the arrival time (relative to the excitation laser pulse) of the photons emitted from the rotor molecules dispersed in the nanoparticles was measured repeatedly. The fluorescence decay curves obtained in this way (Figure 2B, left) were fitted with eq 1, yielding the rotors' fluorescence lifetime. The latter is related to the local viscosity of the environment and thus to the PS concentration in the nanodroplets. In the FCS experiments, the fluctuations of the detected fluorescence intensity, originating from the rotor loaded in nanodroplets diffusing in and out of the confocal volume, were measured to obtain the corresponding autocorrelation curves (Figure 2B, right). The curves were then fitted with eq 3, yielding the diffusion time and thus the hydrodynamic radii of the nanodroplets and nanoparticles.

The fluorescence decay curves (Figure 2B, left) recorded at different time intervals after starting the heating of the miniemulsion were fitted with a biexponential fit (eq 1, i = 2), similar to the cases of the bulk solutions of polystyrene in toluene. Next, the weighted-average lifetime τ_{Av} was calculated with eq 2 and plotted as a function of the heating time (Figure 2C, left). An increase in the molecular rotor lifetime from $\tau_{Av,0\,h}$ = 0.8 ns to $\tau_{Av,6\,h}$ = 4.2 ns with time was observed (Figure 2C, left). The increase originates from the advancing evaporation of the toluene and thus the growing polystyrene concentration and overall viscosity in the nanodroplets.

The simultaneously recorded FCS curves (Figure 2B, right) were fitted with eq 3 to obtain the corresponding diffusion times of the nanodroplets through the confocal observation volume.

A comprehensive picture of the kinetics of nanoparticle formation can be obtained by combining the data of the TCSPC and the FCS experiments (Figure 2B,C). Indeed, by comparing the values of τ_{Av} in the nanodroplets to those measured in polystyrene solutions at various concentrations (Figure 1B), the evolution of the polymer content in the nanodroplets during the emulsion-solvent evaporation process can be estimated (Figure 3, open orange squares). Simultaneously, the FCS data for the diffusion time of the nanodroplets can be used to evaluate the evolution of their size in terms of the hydrodynamic radius (Figure 3, black squares).

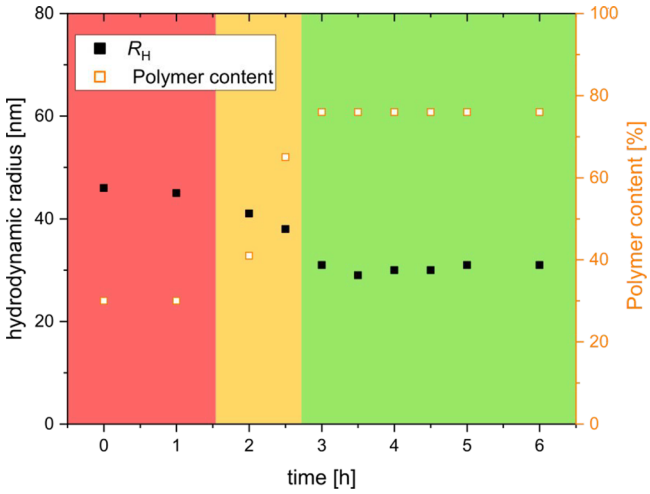

Figure 3. Hydrodynamic radii of the nanoparticles (black squares) and the respective polymer content (open orange squares) vs the emulsion-solvent evaporation process (heating) time. The three stages of the nanoparticle formation process are marked in the graph: solution (red), gel (dark yellow), and the glassy stage (green).

The process of nanoparticles formation by the emulsion solvent evaporation method can be classified in three stages.[51−53] During the first stage, called the "solution stage" (red color in Figure 3), the nanodroplets consisted of diluted (<20%) polymer solution and displayed a relatively large hydrodynamic radius (~46 nm). This stage is characterized by slow evaporation of the toluene through the continuous water phase. The slow evaporation generates a plateau in the observed values of the hydrodynamic radius and the polymer content, which lasts for up to 1.5 h under our experimental conditions. The next stage, the gelation stage (dark-yellow color in Figure 3), was characterized by fast evaporation of the organic solvent from the droplets. The polymer concentration rapidly increased from ~20% to almost 80%, and the particles shrank to a hydrodynamic radius of ~33 nm. During this stage, the structure of the particles started to be stabilized and polymer chains became entangled. Indeed, the entanglement concentration for PS with M_w = 60 kg mol^{-1} was estimated to be 40%.[54] Further solvent evaporation leads to a transition to a glassy stage (green color in Figure 3). Phase separation and the formation of glassy regions (most likely at the outer area of the nanoparticles) hinder the remaining solvent from passing through and slowing down the evaporation process.[53] The formation of a polymer "skin" during the evaporation of a solvent in a confined geometry was observed, for example, in the case of electrospun nanofibers.[55] Again, plateaus for both the polymer concentration and size of the nanoparticles were observed. Even after 6 h, the polymer content in the nanoparticles, as estimated from the molecular rotor lifetime, was still not more than 80%.

To gain a more precise picture of the evolution of the nanoparticles' inner structure during the process, we also monitored the values of the short and long lifetimes and their respective relative amplitudes (Figure 4A,B).

The short lifetime, originating from rotor molecules located in a solvent-rich environment, increased from $\tau_{1,0\,h}$ = 0.7 ns at

https://doi.org/10.1021/acs.macromol.2c01132
Macromolecules 2022, 55, 7284−7293

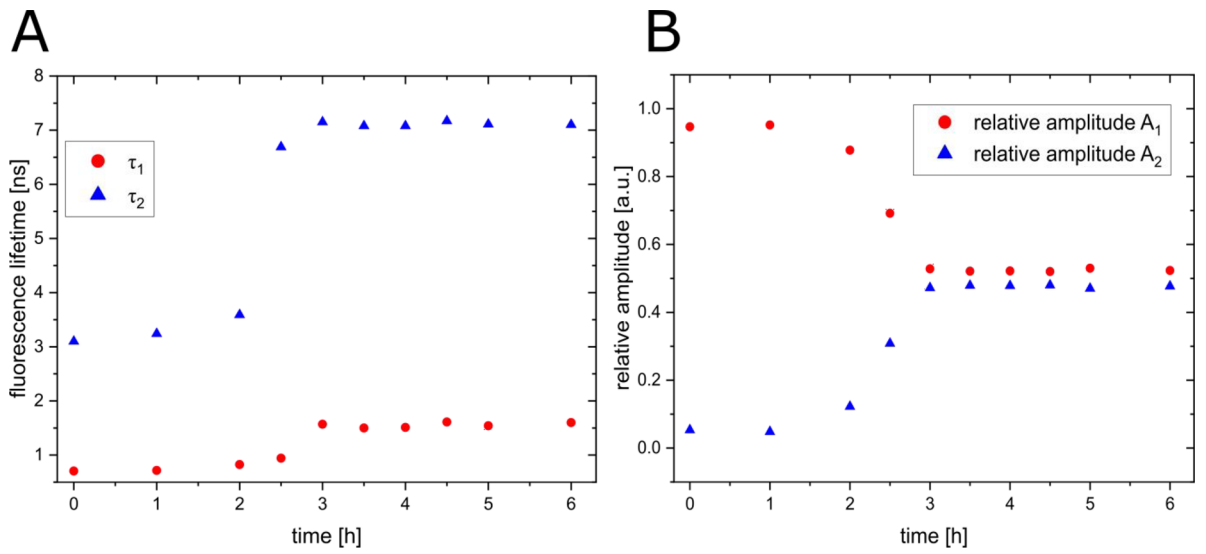

Figure 4. Dependence of (A) the molecular rotor's short and long fluorescence lifetimes and (B) their respective relative amplitudes on the emulsion-solvent evaporation process (heating) time.

the beginning of the process to around $\tau_{1,6\,h}$ = 1.6 ns after 6 h of solvent evaporation, whereas the respective relative amplitudes $A_{1,rel}$ decreased from $A_{1,rel}$ = 95% to around $A_{1,rel}$ = 52%. The long fluorescence lifetime, originating from rotor molecules located in a polymer-rich environment, increased from $\tau_{2,0\,h}$ = 3.1 ns to around $\tau_{2,6\,h}$ = 7.1 ns, and its respective relative amplitudes $A_{2,rel}$ increased from $A_{2,rel}$ = 5% to around $A_{2,rel}$ = 48%. The evolution of the fluorescence lifetimes and their respective amplitudes was caused by the continuous solvent evaporation during the process, leading to an increase in the polymer concentration in the droplets. Thus, the behavior of the molecular rotors in the forming nanoparticles (Figure 4) is qualitatively similar to that observed in bulk polymer solutions with increasing concentrations (Figure S1). In both cases, two fluorescence lifetimes were observed even at very high polystyrene concentrations. Furthermore, in bulk polymer solutions the long lifetime τ_2 reached 6 ns at high polymer concentrations whereas it increased to up to $\tau_{2,6\,h}$ = 7 ns after 6 h of heating in nanoparticles. This high value, repeatedly measured in multiple experiments, can be attributed to the formation of very dense polystyrene regions in the nanoparticles, in which the torsional mobility of the AzeNap1 rotor molecules was even more restricted than in the dry polystyrene films, in which we measure a single fluorescence lifetime of $\tau_{PS\ film}$ = 5.2 ns. The behavior of molecular rotors in polymers is often discussed in terms of the available free volume that affects the torsional mobility.[36,56,57] In these terms, our results indicate that there are regions in the polystyrene nanoparticles in which the free volume is even smaller than in the drop-cast (~5 μm thick) and spin-coated (~500 nm thick) dry polymer films that we studied. It should be noted that a decrease in the free volume or densification was also observed in ultrathin (<100 nm) PS films by means of X-ray reflectivity[58] and magnetic levitation.[59]

Although we observed only one fluorescence lifetime for the AzeNaph1 molecular rotors dispersed in the dry polystyrene films, reflecting the homogeneity of the film, two distinctive lifetimes were observed for the rotors dispersed in the nanoparticles produced by the emulsion solvent evaporation method. Even after 6 h of solvent evaporation, this biexponential behavior persisted, showing that the nanoparticles were still inhomogeneous and contained solvent-rich domains. Moreover, on the basis of the measured value of the relative amplitude of the fast process, it could be estimated that the final nanoparticle consisted of almost 50% of a less-viscous, solvent-rich domains, assuming that the rotor molecules are evenly distributed in solvent-rich and polymer-rich domains.

Additional experiments showed that the solvent-rich domains could not be completely removed even after keeping the nanoparticle dispersion at 40 °C for 24 h. Only after the initial removal of the water phase by drop-casting the dispersion on a glass slide followed by annealing of the dried nanoparticles at 70 °C for 2 h did the fluorescence decay curves of the molecular rotors dispersed in dried nanoparticles become similar to that measured in dry PS films. The curves could be fitted with a monoexponential function, yielding the same lifetime as in dry PS films, i.e., $\tau_{PS\ film}$ = 5.2 ns. Organic solvents employed in the emulsion-solvent evaporation method are typically low-boiling-point solvents such as chloroform, dichloromethane, and ethyl acetate. We therefore performed experiments by replacing toluene with chloroform. The formation of nanoparticles proceeded on a much faster scale (about 1 h compared to 6 h for toluene, Figure S4A) but the behavior of the molecular rotor did not change qualitatively, and two distinct decay times with similar amplitudes (Figure S4B) were detected.

3.3. Polymer Nanoparticles Prepared by Miniemulsion Polymerization. We generalized the concept of monitoring the kinetics of nanoparticle formation with the molecular rotor to another important process for producing polymer nanoparticles, namely, miniemulsion polymerization. In this case, the molecular rotor AzeNaph1 was dissolved, together with a radical initiator and hexadecane as a costabilizer, in styrene. The solution was then emulsified in an aqueous solution of SDS, followed by heating to trigger the thermal initiation of the free-radical polymerization. Aliquots (~250 μL) of the miniemulsion were taken at regular time intervals (0, 10, 20, 30, 40, 50, 60, 90, 120, 180, 240, 300, 360, and 1440 min after sonication) and immediately cooled to prevent further polymerization of styrene. These samples were then investigated with TCSPC and FCS. Typical normalized fluorescence decay curves measured by TCSPC are shown in

https://doi.org/10.1021/acs.macromol.2c01132
Macromolecules 2022, 55, 7284−7293

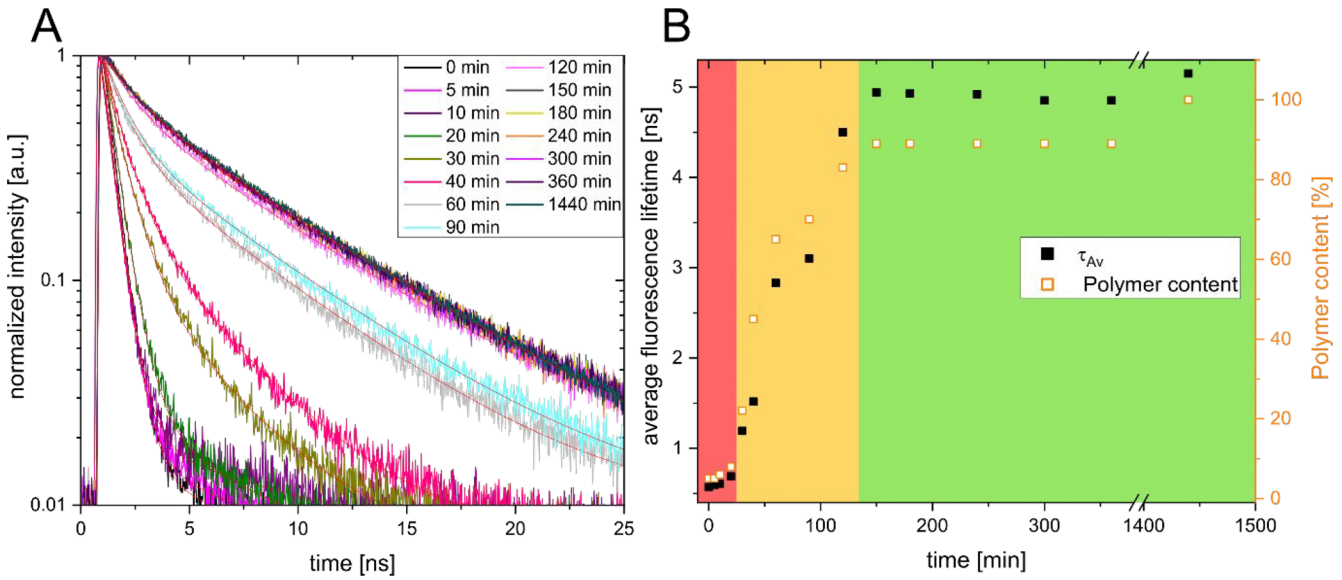

Figure 5. (A) Normalized fluorescence decay curves of the molecular rotors recorded after certain time intervals from the beginning of the miniemulsion polymerization reaction. The curves were fitted (solid lines) using eq 2 (n = 2). (B) Average fluorescence lifetime of the rotors (black squares) and polymer content in the NPs (open orange squares) vs the miniemulsion polymerization reaction (heating) time. The three stages of the nanoparticle formation process are marked in the graph: initiation (red), polymerization (dark yellow), and glassy stage (green).

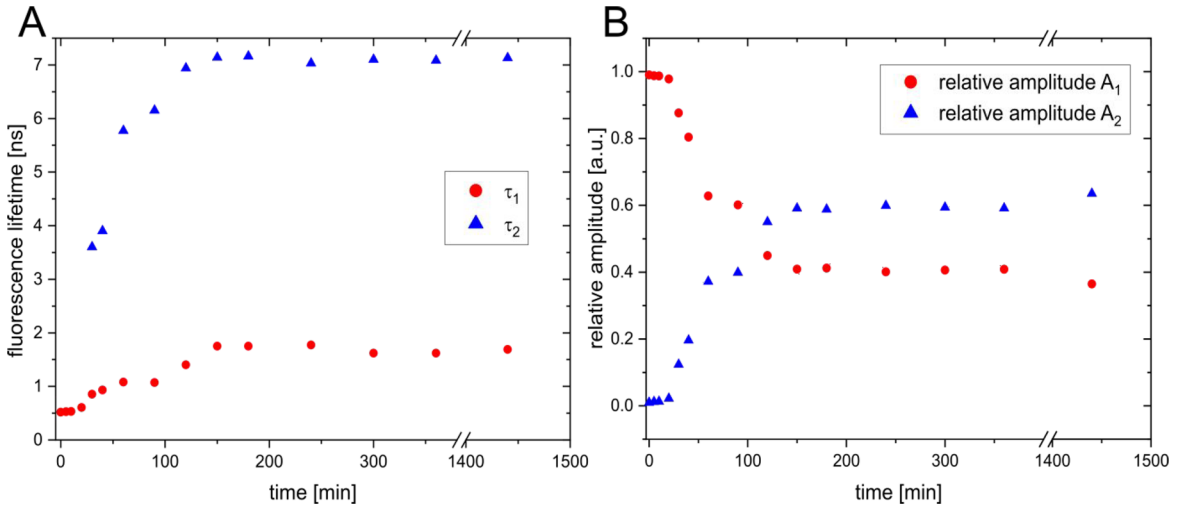

Figure 6. Dependence of (A) the molecular rotor's short and long fluorescence lifetimes and (B) their respective relative amplitudes on the miniemulsion polymerization reaction (heating) time.

Figure 5A. The curves were fitted with a biexponential model (eq 1, n = 2), and then eq 2 was used to obtain the weighted-average lifetime τ_{Av} of the rotor molecules, which is related to the nanodroplets' structure (Figure 5B). FCS experiments performed during the miniemulsion polymerization showed no significant change in the hydrodynamic radius of the nanoparticles (Figure S3). This was expected because the evaporation of styrene through the water phase did not occur because of its high boiling temperature (T_b = 145 °C) and very low solubility in water. Furthermore, the surfactant-stabilized polymerizing styrene nanodroplets were also stable against possible coalescence,[21] which prevented an increase in their size.

Figure 5B summarizes the information provided by the molecular rotor reporters for the kinetics of nanoparticle formation during miniemulsion polymerization by showing the dependence of the weighted-average lifetime of the rotors τ_{Av} (black squares) and the polymer content in the NPs (open orange squares) on polymerization (heating) time. The polymer content was estimated by comparing τ_{Av} measured in the NP dispersion to τ_{Av} measured in bulk solutions of polystyrene in styrene (Figure S2). Even though the particle size did not change during miniemulsion polymerization, their internal structure changed significantly, from low-viscosity styrene (low τ_{Av}) to higher-viscosity polystyrene (high τ_{Av}), and the polymer content increased to around ~90% after 340 min (Figure 5B).

Different stages (Figure 5B) were identified during the miniemulsion polymerization on the basis of the τ_{Av} and polymer content values. The initiation stage (red region in Figure 5B) took place only within the first 20 min of miniemulsion polymerization and is characterized by the fluorescence lifetime of the molecular rotors τ_{Av} on the order of 0.5−0.6 ns. These values are very similar to the ones measured

https://doi.org/10.1021/acs.macromol.2c01132
Macromolecules 2022, 55, 7284−7293

in pure styrene ($\tau_{styrene}$ = 0.5 ns). During the initiation stage, radicals were produced through thermal decomposition of the initiator. The radicals initiated the polymerization of styrene, which led to a transition to the polymerization stage (yellow region in Figure 5B). During this stage, the viscosity of the molecular rotors' environment increased, leading to an increase in their fluorescence lifetimes. The polymer content in the droplets increased from less than 5% to more than 80%. The polymerization stage took place between 30 min to around 120 min and was followed by a third, glassy stage (green color in Figure 5B). The glassy stage was characterized by a plateau in the measured weighted-average lifetime of the molecular rotors, indicating that the polymerization process was completed. The plateau value of around τ_{Av} = 4.8 ns was below the fluorescence lifetime measured in dry polystyrene films $\tau_{PS\ film}$ = 5.2 ns and suggested that ∼90% of the polystyrene was present in the final nanoparticles. Interestingly, fluorescence decay curves recorded after 1440 min showed an even higher fluorescence lifetime of $\tau_{Av,\ 1440\ min}$ = 5.1 ns, indicating that styrene remaining after 340 min was still polymerizing, although very slowly. Although $\tau_{Av,\ 1440\ min}$ = 5.1 ns was almost identical to the fluorescence lifetime measured in dry PS films and thus indicated almost 100% polymer content, it should be noted that the final nanoparticles could not contain more than 95% PS because of the presence of 5% hexadecane. This small discrepancy was most likely related to the heterogeneous nature of the polymer matrix in the final NPs as discussed below.

Besides, the fluorescence decay curves measured in the obtained nanoparticles were fitted with a biexponential function, yielding short and long fluorescence lifetimes. The molecular rotors were still distributed between styrene-rich and polystyrene-rich environments. To further explore these effects, we considered the evolution of the short and long fluorescence lifetimes and their respective amplitudes during the entire miniemulsion polymerization (Figure 6A,B, respectively).

After the short initiation stage (0−20 min), both short and long fluorescence lifetimes increased continuously (Figure 6A) and reached a plateau after ∼120 min. The short lifetime τ_1 increased from 0.5 ns to about 1.7 ns, whereas the long lifetime τ_2 increased from roughly 3.6 ns to about 7 ns. The latter value was higher than the single lifetime measured in bulk PS films (∼5.2 ns) and indicated that similar to the nanoparticles prepared by the emulsion solvent evaporation method, the nanoparticles prepared by miniemulsion polymerization exhibited regions of very high local viscosity. Furthermore, the relative amplitude of the long fluorescence lifetime increased from $A_2 \approx 0\%$ during the initiation phase to around 60% at the end of the polymerization process. Accordingly, the relative amplitude of the fast process A_1 decreased from 100% to roughly 40%, indicating that even in the final NPs about 40% of the AzeNaph1 rotor molecules experienced an environment with a low viscosity. Although this high fraction could be partially affected by the presence of about 5% low-viscosity hexadecane in the final NPs, it should be noted that our results were in accordance with an earlier study by Nölle et al., who reported the fluorescence lifetimes of another molecular rotor, BODIPY-C12, during the free-radical polymerization of MMA in the bulk,[34] which did not involve low-viscosity additives. Indeed, the authors found that even at the end of the reaction (after several days) almost half of the BODIPY-C12 molecules were still in a low-viscosity environment. Although the magnitude of this effect can be influenced by an uneven distribution of the rotor molecules between polymer-rich and monomer-rich environments, the fluorescence lifetime results show that both the bulk polymers studied in ref 34 and the polymer nanoparticles studied here exhibited a significant inhomogeneity on the molecular length scale.[34] Because the molecular rotor lifetime in such dense polymer systems is mainly determined by the available free volume, we conclude that significant variations of the free volume are present even in small (∼100 nm) polystyrene nanoparticles.

4. CONCLUSIONS

We have shown that the formation of polymeric nanoparticles from miniemulsion droplets can be studied with fluorescent molecular rotors. The fluorescent molecular rotor senses the local viscosity inside the particles. By combining fluorescence lifetime analysis and fluorescence correlation spectroscopy, we were able to follow the evolution of the polymer content inside the nanoparticles and their size simultaneously. We applied this approach to the emulsion-solvent evaporation method and miniemulsion polymerization. These are two common methods for preparing polymer nanoparticles. Three stages were identified during the formation of nanoparticles. During the first stage, the viscosity was very low, corresponding to a solvent- or monomer-rich environment in the initial droplets. During the second stage, the polymer content inside the nanoparticles and thus the viscosity increased quickly because of solvent evaporation or polymerization. In the final stage, the weighted-average fluorescence lifetime of the rotors was almost constant and similar to those measured in dry polystyrene films. Because the fluorescence lifetime of a molecular rotor probe is dependent on its local molecular environment, we were able to distinguish significant heterogeneities in the nanoparticles, which were attributed to a remaining solvent and spatial variation in the free volume. The presented experimental approach can hence not only follow the evolution of the polymer content during the emulsion-solvent evaporation and the miniemulsion polymerization processes but also provide valuable information about structural heterogeneities on the molecular length scale. The concept could be further extended in the future to other systems such as internal phase separation between polymer blocks during the formation of block copolymer nanoparticles or the phase separation between an antisolvent and polymer during the formation of polymer nanocapsules.

■ ASSOCIATED CONTENT

Supporting Information

The Supporting Information is available free of charge at https://pubs.acs.org/doi/10.1021/acs.macromol.2c01132.

Additional figures with data on the molecular rotor AzeNaph1 behavior in various environments (PDF)

■ AUTHOR INFORMATION

Corresponding Authors

Roberto Simonutti − *Department of Material Science, University Milano Bicocca, I-20125 Milan, Italy;* orcid.org/0000-0001-8093-517X; Email: roberto.simonutti@unimib.it

Daniel Crespy − *Max Planck-VISTEC Partner Laboratory for Sustainable Materials and Department of Materials Science and Engineering, School of Molecular Science and*

https://doi.org/10.1021/acs.macromol.2c01132
Macromolecules 2022, 55, 7284−7293

Engineering, Vidyasirimedhi Institute of Science and Technology (VISTEC), Rayong 21210, Thailand; orcid.org/0000-0002-6023-703X; Email: daniel.crespy@vistec.ac.th

Kaloian Koynov − *Max Planck Institute for Polymer Research, 55128 Mainz, Germany;* orcid.org/0000-0002-4062-8834; Email: koynov@mpip-mainz.mpg.de

Authors

Sascha Schmitt − *Max Planck Institute for Polymer Research, 55128 Mainz, Germany*

Galit Renzer − *Max Planck Institute for Polymer Research, 55128 Mainz, Germany*

Jennifer Benrath − *Max Planck Institute for Polymer Research, 55128 Mainz, Germany*

Andreas Best − *Max Planck Institute for Polymer Research, 55128 Mainz, Germany*

Shuai Jiang − *Max Planck Institute for Polymer Research, 55128 Mainz, Germany*

Katharina Landfester − *Max Planck Institute for Polymer Research, 55128 Mainz, Germany;* orcid.org/0000-0001-9591-4638

Hans-Jürgen Butt − *Max Planck Institute for Polymer Research, 55128 Mainz, Germany;* orcid.org/0000-0001-5391-2618

Complete contact information is available at: https://pubs.acs.org/10.1021/acs.macromol.2c01132

Funding

This work was funded by the Deutsche Forschungsgemeinschaft (DFG, German Research Foundation) project number 213555243 (SFB 1066 Q02). Open access funded by Max Planck Society.

Notes

The authors declare no competing financial interest.

■ ACKNOWLEDGMENTS

The authors thank Dr. Simone Bonetti for preliminary results and fruitful discussions and Katja Klein for technical assistance with the synthesis. The financial support of the DFG through the SFB 1066 project Q02 is gratefully acknowledged.

■ REFERENCES

(1) You, C. C.; Miranda, O. R.; Gider, B.; Ghosh, P. S.; Kim, I. B.; Erdogan, B.; Krovi, S. A.; Bunz, U. H.; Rotello, V. M. Detection and identification of proteins using nanoparticle-fluorescent polymer 'chemical nose' sensors. *Nat. Nanotechnol* **2007**, *2* (5), 318−323.

(2) Canfarotta, F.; Whitcombe, M. J.; Piletsky, S. A. Polymeric nanoparticles for optical sensing. *Biotechnol Adv.* **2013**, *31* (8), 1585−1599.

(3) Dararatana, N.; Seidi, F.; Crespy, D. pH-Sensitive Polymer Conjugates for Anticorrosion and Corrosion Sensing. *ACS Appl. Mater. Interfaces* **2018**, *10* (24), 20876−20883.

(4) Hou, J.; Li, M.; Song, Y. Recent advances in colloidal photonic crystal sensors: Materials, structures and analysis methods. *Nano Today* **2018**, *22*, 132−144.

(5) Motornov, M.; Roiter, Y.; Tokarev, I.; Minko, S. Stimuli-responsive nanoparticles, nanogels and capsules for integrated multifunctional intelligent systems. *Prog. Polym. Sci.* **2010**, *35* (1−2), 174−211.

(6) Jaroonwatana, W.; Theerathanagorn, T.; Theerasilp, M.; Del Gobbo, S.; Yiamsawas, D.; D'Elia, V.; Crespy, D. Nanoparticles of aromatic biopolymers catalyze CO2 cycloaddition to epoxides under atmospheric conditions. *Sustainable Energy & Fuels* **2021**, *5* (21), 5431−5444.

(7) Astruc, D.; Lu, F.; Aranzaes, J. R. Nanoparticles as recyclable catalysts: the frontier between homogeneous and heterogeneous catalysis. *Angew. Chem., Int. Ed. Engl.* **2005**, *44* (48), 7852−7872.

(8) Jenjob, R.; Phakkeeree, T.; Seidi, F.; Theerasilp, M.; Crespy, D. Emulsion Techniques for the Production of Pharmacological Nanoparticles. *Macromol. Biosci* **2019**, *19* (6), 1900063.

(9) Peer, D.; Karp, J. M.; Farokhzad, S. H. O. C.; Langer, R. M. R. Nanocarriers as an emerging platform for cancer therapy. *Nat. Nanotechnol* **2007**, *2*, 751−760.

(10) Davis, M.; Chen, Z.; Shin, D. Nanoparticle therapeutics: an emerging treatment modality for cancer. *Nat. Rev. Drug Discov* **2008**, *7*, 771−782.

(11) Aricò, A. S.; Bruce, P.; Scrosati, B.; Tarascon, J.-M.; Schalkwijk, W. V. Nanostructured materials for advanced energy conversion and storage devices. *Nature materials* **2005**, *4*, 366−377.

(12) Bannwarth, M. B.; Utech, S.; Ebert, S.; Weitz, D. A.; Crespy, D.; Landfester, K. Colloidal Polymers with Controlled Sequence and Branching Constructed from Magnetic Field Assembled Nanoparticles. *ACS Nano* **2015**, *9* (3), 2720−2728.

(13) Duguet, E.; Desert, A.; Perro, A.; Ravaine, S. Design and elaboration of colloidal molecules: an overview. *Chem. Soc. Rev.* **2011**, *40* (2), 941−960.

(14) Bai, L.; Mai, V. C.; Lim, Y.; Hou, S.; Mohwald, H.; Duan, H. Large-Scale Noniridescent Structural Color Printing Enabled by Infiltration-Driven Nonequilibrium Colloidal Assembly. *Adv. Mater.* **2018**, *30* (9), 1705667.

(15) Hou, J.; Li, M.; Song, Y. Patterned Colloidal Photonic Crystals. *Angew. Chem., Int. Ed. Engl.* **2018**, *57* (10), 2544−2553.

(16) Isapour, G.; Lattuada, M. Bioinspired Stimuli-Responsive Color-Changing Systems. *Adv. Mater.* **2018**, *30* (19), 1707069.

(17) Jenjob, R.; Seidi, F.; Crespy, D. Recent advances in polymerizations in dispersed media. *Adv. Colloid Interface Sci.* **2018**, *260*, 24−31.

(18) Staff, R. H.; Landfester, K.; Crespy, D. *Hierarchical Macromolecular Structures: 60 Years after the Staudinger Nobel Prize*; Percec, V., Ed.; Springer: Cham, Switzerland, 2013; Vol. *2*.

(19) Crespy, D.; Landfester, K. Miniemulsion polymerization as a versatile tool for the synthesis of functionalized polymers. *Beilstein J. Org. Chem.* **2010**, *6*, 1132−1148.

(20) Staff, R. H.; Schaeffel, D.; Turshatov, A.; Donadio, D.; Butt, H. J.; Landfester, K.; Koynov, K.; Crespy, D. Particle formation in the emulsion-solvent evaporation process. *Small* **2013**, *9* (20), 3514−3522.

(21) Schaeffel, D.; Staff, R. H.; Butt, H. J.; Landfester, K.; Crespy, D.; Koynov, K. Fluorescence correlation spectroscopy directly monitors coalescence during nanoparticle preparation. *Nano Lett.* **2012**, *12* (11), 6012−6017.

(22) Gharieh, A.; Khoee, S.; Mahdavian, A. R. Emulsion and miniemulsion techniques in preparation of polymer nanoparticles with versatile characteristics. *Adv. Colloid Interface Sci.* **2019**, *269*, 152−186.

(23) Landfester, K. Recent developments in miniemulsions —— formation and stability mechanisms. *Macromelecular Symposia* **2000**, *150*, 171−178.

(24) Haidekker, M. A.; Brady, T. P.; Lichlyter, D.; Theodorakis, E. A. Effects of solvent polarity and solvent viscosity on the fluorescent properties of molecular rotors and related probes. *Bioorg Chem.* **2005**, *33* (6), 415−425.

(25) Haidekker, M. A.; Theodorakis, E. A. Environment-sensitive behavior of fluorescent molecular rotors. *J. Biol. Eng.* **2010**, *4*, 11.

(26) Vyšniauskas, A.; Kuimova, M. K. A twisted tale: measuring viscosity and temperature of microenvironments using molecular rotors. *Int. Rev. Phys. Chem.* **2018**, *37* (2), 259−285.

(27) Polita, A.; Toliautas, S.; Zvirblis, R.; Vysniauskas, A. The effect of solvent polarity and macromolecular crowding on the viscosity sensitivity of a molecular rotor BODIPY-C10. *Phys. Chem. Chem. Phys.* **2020**, *22* (16), 8296−8303.

(28) Kuimova, M. K. Molecular rotors image intracellular viscosity. *Chimia (Aarau)* **2012**, *66* (4), 159−165.
(29) Kuimova, M. K.; Yahioglu, G.; Levitt, J. A.; Suhling, K. Molecular Rotor Measures Viscosity of Live Cells via Fluorescence Lifetime Imaging. *J. Am. Chem. Soc.* **2008**, *130*, 6672−6673.
(30) Kuimova, M. K. Mapping viscosity in cells using molecular rotors. *Phys. Chem. Chem. Phys.* **2012**, *14* (37), 12671−12686.
(31) Jungst, C.; Klein, M.; Zumbusch, A. Long-term live cell microscopy studies of lipid droplet fusion dynamics in adipocytes. *J. Lipid Res.* **2013**, *54* (12), 3419−3429.
(32) Levitt, J. A.; Kuimova, M. K.; Yahioglu, G.; Chung, P. H.; Suhling, K.; Phillips, D. Membrane-Bound Molecular Rotors Measure Viscosity in Live Cells via Fluorescence Lifetime Imaging. *J. Phys. Chem. C* **2009**, *113*, 11634−11642.
(33) Vaccaro, G.; Bianchi, A.; Mauri, M.; Bonetti, S.; Meinardi, F.; Sanguineti, A.; Simonutti, R.; Beverina, L. Direct monitoring of self-assembly of copolymeric micelles by a luminescent molecular rotor. *Chem. Commun. (Camb)* **2013**, *49* (76), 8474−8476.
(34) Nölle, J. M.; Jüngst, C.; Zumbusch, A.; Wöll, D. Monitoring of viscosity changes during free radical polymerization using fluorescence lifetime measurements. *Polym. Chem.* **2014**, *5* (8), 2700−2703.
(35) Jbilou, F.; Georgousopoulou, I.-N.; Marinkovic, S.; Vouyiouka, S.; Papaspyrides, C. D.; Estrine, B.; Dole, P.; Cottaz, A.; Joly, C. Intelligent monitoring of solid state polymerization via molecular rotors: The case of poly(butylene succinate). *Eur. Polym. J.* **2016**, *78*, 61−71.
(36) Loutfy, R. O. Fluorescence probes for polymer free-volume. *Pure Appl. Chem.* **1986**, *58* (9), 1239−1248.
(37) Papadakis, C. M.; Košovan, P.; Richtering, W.; Wöll, D. Polymers in focus: fluorescence correlation spectroscopy. *Colloid Polym. Sci.* **2014**, *292* (10), 2399−2411.
(38) Koynov, K.; Butt, H.-J. Fluorescence correlation spectroscopy in colloid and interface science. *Curr. Opin. Colloid Interface Sci.* **2012**, *17* (6), 377−387.
(39) Zhao, J.; Granick, S. Polymer Lateral Diffusion at the Solid-Liquid Interface. *J. Am. Chem. Soc* **2004**, *126*, 6242−6243.
(40) Bosco, S. J.; Zettl, H.; Crassous, J. J.; Ballauff, M.; Krausch, G. Interactions between Methyl Cellulose and Sodium Dodecyl Sulfate in Aqueous Solution Studied by Single Molecule Fluorescence Correlation Spectroscopy. *Macromolecules* **2006**, *39* (25), 8793−8798.
(41) Omari, R. A.; Aneese, A. M.; Grabowski, C. A.; Mukhopadhyay, A. Diffusion of Nanoparticles in Semidilute and Entangled Polymer Solutions. *J. Phys. Chem. B* **2009**, *113* (25), 8449−8452.
(42) Szymanski, J.; Weiss, M. Elucidating the origin of anomalous diffusion in crowded fluids. *Phys. Rev. Lett.* **2009**, *103* (3), 038102. From NLM Medline.
(43) Zettl, U.; Hoffmann, S. T.; Koberling, F.; Krausch, G.; Enderlein, J.; Harnau, L.; Ballauff, M. Self-Diffusion and Cooperative Diffusion in Semidilute Polymer Solutions As Measured by Fluorescence Correlation Spectroscopy. *Macromolecules* **2009**, *42* (24), 9537−9547.
(44) Dorfschmid, M.; Müllen, K.; Zumbusch, A.; Wöll, D. Translational and Rotational Diffusion during Radical Bulk Polymerization: A Comparative Investigation by Full Correlation Fluorescence Correlation Spectroscopy (fcFCS). *Macromolecules* **2010**, *43* (14), 6174−6179.
(45) Ochab-Marcinek, A.; Hołyst, R. Scale-dependent diffusion of spheres in solutions of flexible and rigid polymers: mean square displacement and autocorrelation function for FCS and DLS measurements. *Soft Matter* **2011**, *7* (16), 7366.
(46) Zhang, X.; Yager, K. G.; Kang, S.; Fredin, N. J.; Akgun, B.; Satija, S.; Douglas, J. F.; Karim, A.; Jones, R. L. Solvent Retention in Thin Spin-Coated Polystyrene and Poly(methyl methacrylate) Homopolymer Films Studied By Neutron Reflectometry. *Macromolecules* **2010**, *43* (2), 1117−1123.
(47) Lee, S. C.; Heo, J.; Woo, H. C.; Lee, J. A.; Seo, Y. H.; Lee, C. L.; Kim, S.; Kwon, O. P. Fluorescent Molecular Rotors for Viscosity Sensors. *Chemistry* **2018**, *24* (52), 13706−13718.
(48) Miao, W.; Yu, C.; Hao, E.; Jiao, L. Functionalized BODIPYs as Fluorescent Molecular Rotors for Viscosity Detection. *Front Chem.* **2019**, *7*, 825.
(49) Amdursky, N.; Erez, Y.; Huppert, D. Molecular Rotors: What Lies Behind the High Sensitivity of the Thioflavin-T Fluorescent Marker. *Acc. Chem. Res.* **2012**, *45*, 1548−1557.
(50) Bohlender, C.; Landfester, K.; Crespy, D.; Schiller, A. Unconventional Non-Aqueous Emulsions for the Encapsulation of a Phototriggerable NO-Donor Complex in Polymer Nanoparticles. *Particle & Particle Systems Characterization* **2013**, *30* (2), 138−142.
(51) Li, W.-I.; Anderson, K. W.; Mehta, R. C.; DeLuca, P. P. Prediction of solvent removal profile and effect on properties for peptide-loaded PLGA microspheres prepared by solvent extraction/evaporation method. *J. Controlled Release* **1995**, *37*, 199−214.
(52) Li, W.-I.; Anderson, K. W.; DeLuca, P. P. Kinetic and thermodynamic modeling of the formation of polymeric microspheres using solvent extraction/evaporation method. *J. Controlled Release* **1995**, *37*, 187−198.
(53) *Polymer Nanoparticles for Nanomedicines*; Vauthier, C., Ponchel, G., Eds.; Springer International, 2016. .
(54) Colby, R. H. Structure and linear viscoelasticity of flexible polymer solutions: comparison of polyelectrolyte and neutral polymer solutions. *Rheol. Acta* **2010**, *49* (5), 425−442.
(55) Reneker, D. H.; Yarin, A. L. Electrospinning jets and polymer nanofibers. *Polymer* **2008**, *49* (10), 2387−2425.
(56) Jee, A.-Y.; Bae, E.; Lee, M. Internal Twisting Dynamics of Dicyanovinyljulolidine in Polymers. *J. Phys. Chem. B* **2009**, *113*, 16508−16512.
(57) Zhu, D.; Haidekker, M. A.; Lee, J.-S.; Won, Y.-Y.; Lee, J. C.-M. Application of Molecular Rotors to the Determination of the Molecular Weight Dependence of Viscosity in Polymer Melts. *Macromolecules* **2007**, *40*, 7730−7732.
(58) Vignaud, G.; M, S. C.; Bal, J. K.; Delorme, N.; Beuvier, T.; Grohens, Y.; Gibaud, A. Densification and depression in glass transition temperature in polystyrene thin films. *Langmuir* **2014**, *30* (39), 11599−11608.
(59) Root, S. E.; Gao, R.; Abrahamsson, C. K.; Kodaimati, M. S.; Ge, S.; Whitesides, G. M. Estimating the Density of Thin Polymeric Films Using Magnetic Levitation. *ACS Nano* **2021**, *15* (10), 15676−15686.

https://doi.org/10.1021/acs.macromol.2c01132
Macromolecules 2022, 55, 7284−7293